

Article title: The first order statistics of backscatter from the fractal branching vasculature

Authors: Kevin J. Parker^{a)}
Department of Electrical and Computer Engineering, University of Rochester, Rochester, New York 14627, USA

Date: 05/29/2019

Running title: The first order statistics of backscatter from the fractal branching vasculature

^{a)} Author to whom correspondence should be addressed. Electronic mail: kevin.parker@rochester.edu

ABSTRACT

The issue of speckle statistics from ultrasound images of soft tissues such as the liver has a long and rich history. A number of theoretical distributions, some related to random scatterers or fades in optics and radar, have been formulated for pulse-echo interference patterns. This work proposes an alternative framework in which the dominant echoes are presumed to result from Born scattering from fluid filled vessels that permeate the tissue parenchyma. These are modeled as a branching, fractal, self-similar, multi scale collection of cylindrical scatterers governed by a power law distribution relating the number of branches at each radius. A deterministic accounting of the echo envelopes across the scales from small to large is undertaken, leading to a closed form theoretical formula for the histogram of the envelope of the echoes. The histogram is found to be governed by the power law distribution of the cylindrical weak scatterers. Examples are given from liver scans to demonstrate the applicability of the theory.

I. INTRODUCTION

A century of research on scattering of light and sound has accumulated since the landmark papers of Rayleigh (Rayleigh, 1897; 1918a) and today, every day, an uncountable number of ultrasound scans are created from tissue backscatter. In normal, soft tissues such as the liver, prostate, and thyroid, the source of the backscatter is presumed to be internal inhomogeneities which have been typically modelled as spherical shapes linked to the cellular structures of the soft tissue. A recently proposed alternative hypothesis is that within soft and macroscopically isotropic tissues such as the liver, the dominant parenchymal cellular structure forms the *reference media* and the fractal branching vasculature and fluid channels form the *weak scattering structures* within the Born approximation. The consequences of this new framework are significant, as the canonical structural shape must be cylindrical, not spherical, and the self-similar or fractal or multi-scale nature of the branching fluid channels must be considered within the ensemble average.

The second order statistics, specifically the ensemble-averaged backscatter, has been recently considered for this new hypothesis (Parker, 2019; Parker *et al.*, 2019), and the fractal branching cylindrical models were found to predict a power law (f^γ) increase in backscatter vs. frequency for tissues such as the liver, matching the experimental results from the early leading studies (Campbell and Waag, 1984; Zagzebski *et al.*, 1993).

However, the first order statistics of soft tissues under the new hypothesis have not yet been resolved. The distribution of the envelope of echoes from the liver and other soft tissues has been an intense subject of research over the years (Burckhardt, 1978; Bamber and Dickinson, 1980; Sleaf and Lele, 1988; Landini and Verrazzani, 1990; Wear *et al.*, 1997; Cramblitt and Parker, 1999; Kutay *et al.*, 2001; 2003; Laporte *et al.*, 2009). Based on models originating from

radar and optical speckle, and on 1D convolution models, the envelope of RF echoes have been fit to Rayleigh, Gamma, Rician, Homodyne-K, and other distributions. It was hoped that some measure of tissue structure, such as the number of discrete scatterers per unit volume, could be estimated from these distribution functions.

In this analysis we depart from these frameworks in two significant ways: first, the scattering structures are assumed to be a multiscale set of cylindrical vessels of radius a with a density distribution that follows a power law, $N(a) = N_0/a^b$. Secondly, we derive a fully deterministic (not probabilistic) ensemble of echo amplitudes based on the dominant (maximum) signals obtained from the 3D convolution of a pulse with the isotropic ensemble of scattering cylindrical vessels. The result is a model of the envelope histogram that is deterministic and somewhat resembles – but is not equal to – the Rayleigh distribution. In this framework a key tissue parameter of the envelope distribution is the power law parameter b , which captures the multi-scale distribution of vessels from the few large vessels to the greater numbers of smaller vessels.

II. THEORY

Assume a broadband pulse propagating in the x direction is given by separable functions:

$$P\left(y, z, t - \frac{x}{c}\right) = G_y(y, \sigma_y) G_z(z, \sigma_z) P_x\left(t - \frac{x}{c}\right), \quad (1)$$

where $G_y(y, \sigma_y) = \exp[-y^2/2\sigma_y^2]$, i.e., Gaussian in the y and z directions, and where the pulse shape P_x in the x direction is given by:

$$P_x(x) = GH_2\left(\frac{x}{\sigma_x}\right) \exp\left(-\frac{x}{\sigma_x}\right)^2 = \mathbf{e}^{-x^2/\sigma_x^2} \left(\frac{4x^2}{\sigma_x^2} - 2\right), \quad (2)$$

where GH_2 is a second-order Hermite polynomial for the pulse shape with a spatial scale factor of σ_x (Poularikas, 2010; Parker, 2016), representing a broadband pulse. Its spatial Fourier transform is then:

$${}^{3D}\mathfrak{F}\{P(x, y, z, t=0)\} = \left(4e^{-k_x^2\pi^2\sigma_x^2}k_x^2\pi^{5/2}\sigma_x^3\right)\left(e^{-2k_y^2\pi^2\sigma_y^2}\sqrt{2\pi}\sigma_y\right)\left(e^{-2k_z^2\pi^2\sigma_z^2}\sqrt{2\pi}\sigma_z\right), \quad (3)$$

where we use Bracewell's convention (1965b) for the form of the Fourier transform.

Using a 3D convolution model (Bamber and Dickinson, 1980; Macovski, 1983; Prince and Links, 2015), we will determine the *dominant* echoes from the pulse interacting with each generation of elements in a branching, fractal, self-similar set of vessels shown in **Figure 1**, and whose number density follows a power law behavior $N(a) = N_0/a^b$. From these echoes, the histogram of envelopes is determined, by summing up over all the fractal branches.

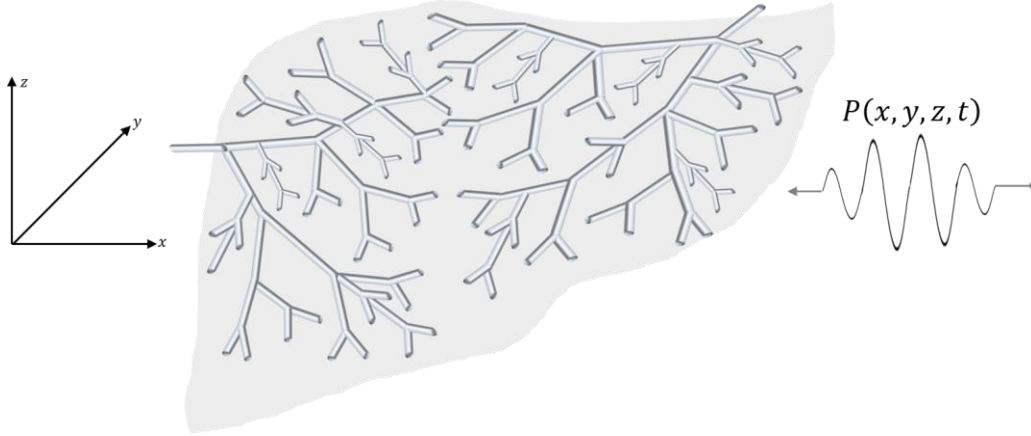


Figure 1. Model of 3D convolution of a pulse with the fractal branching cylindrical fluid-filled channels in a soft tissue.

Assuming an isotropic spatial and angular distribution of each generation of fractal branching structures, we need to consider a basic element across all angles of incidence with respect to the propagating wave and across all size scales, from very small micro channels of flu-

id to the largest arteries and veins that can exist within the organ. Specifically, we will examine a long fluid-filled cylinder of radius a :

$$\begin{aligned} f(r) &= \begin{cases} \kappa_0 & r \leq a \\ 0 & r > a \end{cases} \\ F(\rho) &= \frac{\kappa_0 \cdot a \cdot J_1[2\pi a \cdot \rho]}{\rho}, \end{aligned} \tag{4}$$

where κ_0 is the fractional variation in compressibility and density, assumed to be $\ll 1$ consistent with the Born formulation, $F(\rho)$ represents the Hankel transform, which is the 2D Fourier transform of a radially symmetric function, $J_1[\cdot]$ is a Bessel function of order 1, and ρ is the spatial frequency. The fractional variation in compressibility, κ_0 , between blood vessels and liver parenchyma has been estimated to be approximately 0.03, or a 3% difference based on published data (Parker, 2019).

Consider first one infinitely long cylinder with material property $f(r)$ – symmetric – as shown in **Figure 2(a)** and tilted at some arbitrary angle in a spherical coordinate system. It has a 3D transform that is a thin disk, shown in **Figure 2(b)** (delta function k_z but shown with finite thickness to make the graphic easier to draw and visualize). A particular radius of spatial frequency equal to q_0 is shown for reference. The shape of the 3D spatial Fourier transform of the pulse is shown in **Figure 2(c)**.

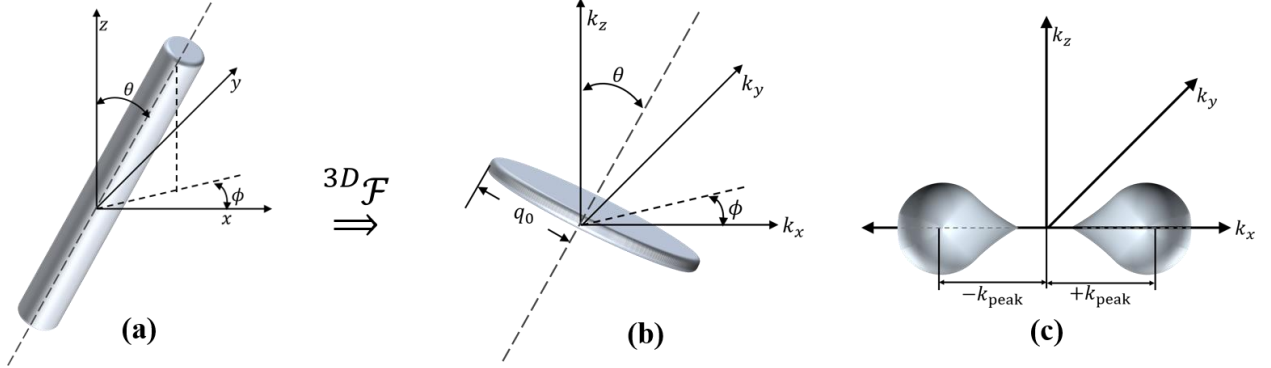


Figure 2. A cylindrical function (a) and its Hankel transform represented in 3D Fourier transform space (b). Rotations around spherical coordinates similarly rotates the corresponding transform. The transform of a propagating pulse is shown in (c). The maximum product of (b) and (c) arrives when the angle θ approaches zero.

One can see from **Figure 2** that, the convolution of the pulse with a cylinder of radius a is dominated by the case where the cylinder is perpendicular to the direction of the forward propagating pulse, the x -axis in our case. For all other orientations, the delta function of the cylindrical transform shown in **Figure 2(a)** is misaligned with respect to the transform of the pulse shown in **Figure 2(c)**. Thus, assuming an optimal alignment, the 3D convolution result is given by the product of the transforms:

$$\begin{aligned}
 {}^{3D}\mathfrak{T}\{echo(t)\} &= \mathfrak{T}^{3D}\{p(x, y, z, t=t_0)\} \cdot (k_x)^2 \mathfrak{T}^{3D}\{cylinder(x, y, z)\} = \\
 &\left(\left(4e^{-k_x^2 \pi^2 \sigma_x^2} k_x^2 \pi^{5/2} \sigma_x^3 \right) \left(e^{-2k_y^2 \pi^2 \sigma_y^2} \sqrt{2\pi} \sigma_y \right) \left(e^{-2k_z^2 \pi^2 \sigma_z^2} \sqrt{2\pi} \sigma_z \right) \right) \cdot \\
 &(k_x)^2 \kappa_0 \left(a \left[\frac{1}{\sqrt{k_x^2 + k_y^2}} \right] \cdot \left(J_1 \left[1, 2a\pi \sqrt{k_x^2 + k_y^2} \right] \right) \right) \delta[k_z],
 \end{aligned} \tag{5}$$

where the $(k_x)^2$ term pre-multiplying the cylinder transform stems from the Laplacian spatial derivative in the Born scattering formulation (Rayleigh, 1918a; Morse and Ingard, 1987) and in the 3D convolution model (Gore and Leeman, 1977; Bamber and Dickinson, 1980).

By Parseval's theorem, the integral of the square of the transform equals the integral of the square of the echo, and after integration over the delta function in k_z :

$$\int (\text{echo}(t))^2 dt = \sigma_z \kappa_0^2 \int_{k_x=0}^{\infty} \int_{k_y=0}^{\infty} \left(8e^{-\pi^2(k_x^2\sigma_x^2+2k_y^2\sigma_x^2)} k_x^2 \pi^3 \sigma_x^3 \sigma_y \right)^2 \cdot (k_x)^2 \left(a \left[\frac{1}{\sqrt{k_x^2 + k_y^2}} \right] \cdot \left(J_1 \left[2a\pi\sqrt{k_x^2 + k_y^2} \right] \right) \right)^2 dk_x dk_y. \quad (6)$$

The square root of this gives the root mean square (RMS) amplitude of the echo, as a function of the radius a , shown for the practical span of $0 < a < 10$ in **Figure 3**. We will associate the RMS amplitude from each echo with a proportionally higher maximum value of the envelope, as a function of cylinder radius a . This single value mapping is justified in the **Appendix**.

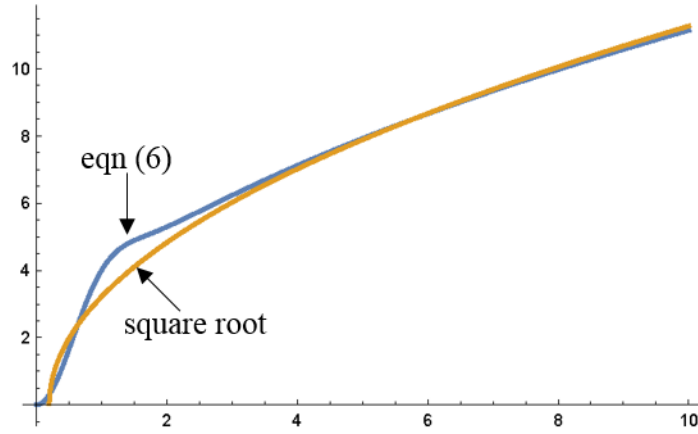


Figure 3. The RMS echo amplitude (vertical axis, arbitrary units) vs. cylinder radius from eqn (6), and square root approximation, assuming a GH_2 pulse.

Also shown in **Figure 3** is an approximation which will be useful for deriving a closed form solution, the approximation is of the form $A[a] = A_0 \sqrt{a - a_{\min}}$, justified by the nearly linear increase in the energy term above some minimum threshold, and the asymptotic modulus of $J_1(ak)$ which is proportional to $\sqrt{2/(\pi ak)}$ (Abramowitz and Stegun, 1964) as ak becomes large. Of course the exact shape is dependent on the particular pulse shape's spectrum, for example if instead of a GH_2 we use a $k_x \cdot \text{sech}[k_x]$ bandpass for $\Im\{P_x(x)\}$, which has an exponential asymptotic tail instead of a Gaussian, then the result is shown in **Figure 4**:

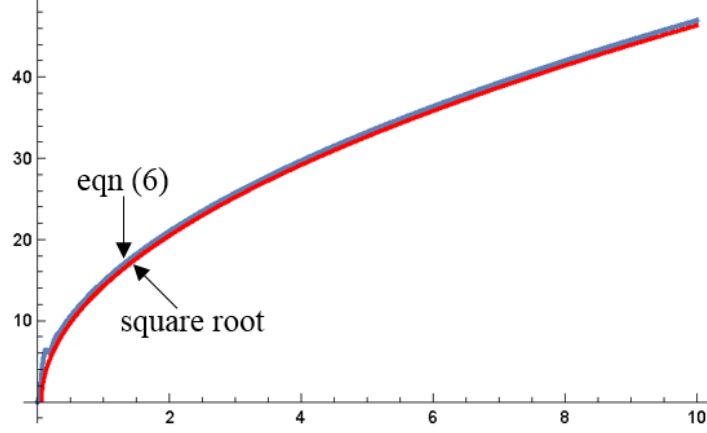


Figure 4. The RMS echo amplitude for a second pulse shape vs. radius of a scattering cylinder, and a root square approximation.

So as a general approximation, we apply the relation $A[a] = A_0 \sqrt{a - a_{\min}}$ for $a > a_{\min}$. The parameter a_{\min} depends on a number of factors, including the dynamic range selected (for example, 45 dB) and the Rayleigh scattering (long wavelength, small a) behavior of the cylinder interacting with the particular pulse transmit signal, along with the noise floor and quantization floor of the receiver.

Now, applying the general theory of transformed distributions (see **Appendix**), we have within the ensemble the number density of vessels at different radii given by $N[a] = N_0/a^b$, and this will be transformed into the distribution of amplitudes, $A(a)$. The general rule is:

$$N[A] = \frac{1}{dA/da} N[a] \quad (7)$$

In our case, the derivative $dA/da = [(1/2)A_0]/\sqrt{a - a_{\min}}$, and the inverse function is

$a[A] = (A/A_0)^2 + a_{\min}$. Thus, substituting these into eqn (7) the distribution $N[A]$ is:

$$N[A] = \frac{2N_0A/A_0}{\left[(A/A_0)^2 + a_{\min}\right]^b} \quad (8)$$

So, for example, if $b = 2$ and A_0 and N_0 are unity, then $N[a] = 2A/(A^2 + a_{\min})^2$, and this is plotted in **Figure 5** along with variations in parameters.

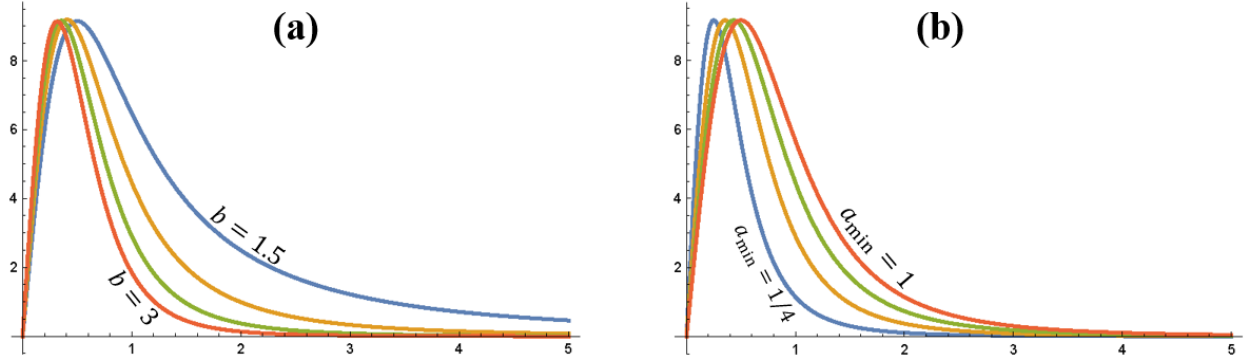


Figure 5. The proposed histogram function of envelope amplitudes A , having the form $A/(A + a_{\min})^b$. In (a) are normalized functions where $a_{\min} = 1/2$ and the power law parameter b is 3, 2.5, 2, and 1.5. In (b) are normalized functions where the power law parameter is fixed at 2.5 however a_{\min} is varied as 1/4, 1/2, 3/4, and 1. Vertical axis: counts (arbitrary units); horizontal axis: envelope amplitude (arbitrary units).

This provides a four-parameter fit $\{N_0, A_0, a_{\min}, b\}$ to a histogram taken from a reasonably sized region of interest (ROI) within a vascularized tissue or organ, assuming an isotropic and spatially uniform distribution across the ROI.

Using the notations from Bracewell (1965a), we calculate by integration the centroid of the distribution and find the expected value of the histogram:

$$\langle A \rangle = \frac{A_0 \sqrt{a_{\min}} (-1+b) \sqrt{\pi} \Gamma \left[-\frac{3}{2} + b \right]}{2 \Gamma [b]}, \quad (9)$$

where $\Gamma[\cdot]$ is the gamma function (Abramowitz and Stegun, 1964). Similarly, the mean square abscissa can found by integration:

$$\langle A^2 \rangle = \frac{2A_0^2 a_{\min} (-1+b)}{4 - 6b + 2b^2} \quad \text{for } b > 2. \quad (10)$$

In a similar way, the variance can be calculated, and then a measure of signal-to-noise (ratio, SNR) defined by the mean value over the standard deviation is:

$$\text{SNR} = \frac{\langle A \rangle}{\sigma_A} = \frac{\frac{(-1+b)\pi^{3/2}\Gamma\left[-\frac{3}{2}+b\right]}{2\Gamma[b]}}{\sqrt{\frac{1}{4}\pi^2\left(\frac{4\pi}{A_0(-2+b)} + \frac{(A_0-2\pi)\Gamma\left[-\frac{3}{2}+b\right]^2}{\Gamma(-1+b)^2}\right)}}. \quad (11)$$

Generally, in the range of interest ($2 < b < 4$ and $A_0 > 10$), we find that the SNR is less than 1.6, which is below the theoretical 1.91 SNR found for fully-developed speckle under a Rayleigh probability density function (Burckhardt, 1978; Tuthill *et al.*, 1988; Thijssen, 2003). However, it must be kept in mind that our underlying model of cylinders vs. radius has a power law tail as the radius a goes to infinity, creating a long asymptotic tail of high amplitude. In practice, each organ has a finite upper limit to the largest artery or vein, and this truncates the upper tail of the distribution, leading to a smaller standard deviation and a larger SNR than would be suggested by formulas.

III. METHODS

In the following examples, conventional B-scans were obtained using a Verasonics scanner with a 5 MHz ATL linear array transducer (V1, Verasonics, Inc., Kirkland, WA, USA). A scan from a healthy adult was imaged under the requirements of informed consent and the University of Rochester Institutional Review Board. Rat experiments were reviewed and approved by the Institutional Animal Care and Use Committee of Pfizer, Inc. Groton Connecticut, where

the ultrasound scan was acquired using a Vivo 2100 (VisualSonics, Toronto, CA) scanner and a 20 MHz center frequency transducer (data provided courtesy of Terry Swanson).

IV. RESULTS

An ultrasound B-scan of a normal rat liver is shown in **Figure 6 (left)**, with a region of interest denoted within the liver parenchyma where the pattern of echoes demonstrates a speckle pattern. This region is distal to the transmit focus, which is located at 11 mm depth. A close-up view is shown in **Figure 6 (right)**.

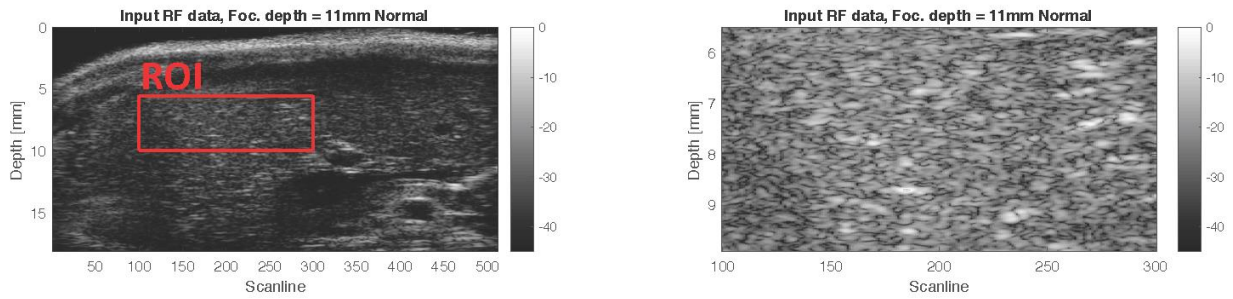


Figure 6. Left: ultrasound B-scan image from a 20 MHz scan of a normal rat liver, focused transmit at 11 mm depth. Right: zoom view of speckle region ROI selected for analysis.

The envelope of the beam formed RF is distributed as shown in the histogram of **Figure 7**, along with a theoretical curve with a power law parameter of $b = 2.7$. The match of this deterministic theory to the data is reasonable.

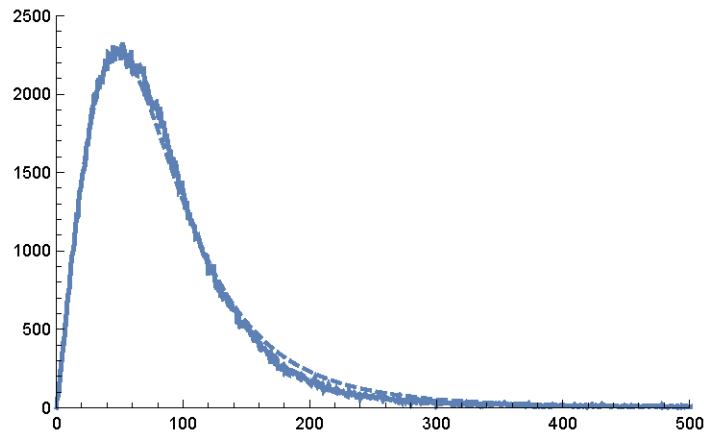


Figure 7. Histogram of echo amplitudes from the normal rat liver. Vertical axis = counts; horizontal axis = amplitudes of echo envelopes (arbitrary units). The dashed line indicates theoretical fit to the derived eqn (8), with the power law parameter of $b = 2.7$ and $a_{\min} = 6.9$.

The normal human liver is shown in **Figure 8**. This utilized five compounded plane wave transmit pulses with dynamic receive.

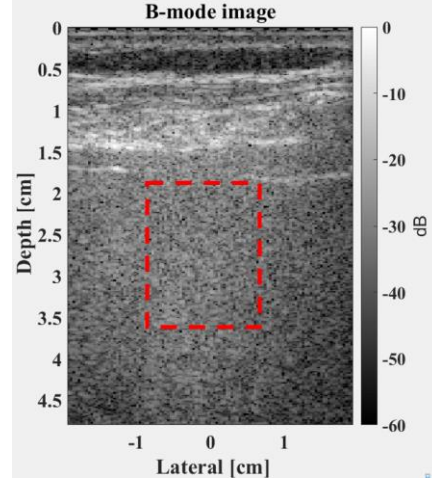


Figure 8. B-scan image of healthy liver tissue in a human. A region of interest is selected (dotted lines) for analysis.

The histogram of echo amplitudes is shown in **Figure 9** along with the theoretical curve fit with a power law parameter of $b = 2.2$.

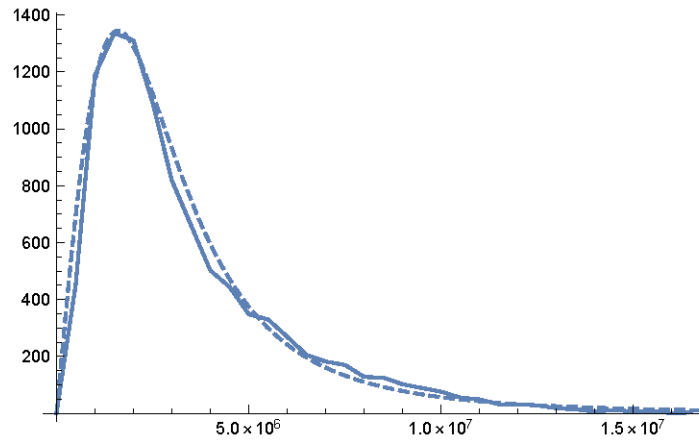


Figure 9. Data from a 5 MHz probe on a normal human liver with $b = 2.2$ and $a_{\min} = 2.4$. Vertical axis: counts; horizontal axis: amplitudes of echo envelopes (arbitrary units).

V. DISCUSSION AND CONCLUSION

This framework postulates that the histogram of speckle amplitudes is governed by a simple equation eqn (8) governed by four parameters: a power law b , a minimum cylinder size a_{\min} above which the echo amplitude rises as a square root of radius, a vessel density N_0 , and a scale amplitude A_0 depending on system factors such as amplifier gain. The formulation is a major departure from the treatments over the last 100 years in that the accounting is deterministic and focused on the maximum or predominant result in each step. Effectively, this means that each local maximum of the echoes is modeled as resulting from one dominant cylinder aligned perpendicular to the propagation direction of the pulse. Then, assuming a spatial ensemble large enough to encompass all radii according to the power law, the form of eqn (8) is derived as the histogram of speckle envelopes within soft vascularized tissue. This formulation is limited by the major assumptions which simplify the derivations:

- The echoes are assumed to be produced by long cylindrical fluid-filled Born scatterers, dominated by those cylinders that are aligned perpendicular to the propagating pulse.
- The echoes from each generation of cylinders of radius a are mapped to an envelope amplitude of A by a square root function.
- The local maxima of envelopes dominate the histogram of sampled echoes.

Each of these assumptions are linked to a theoretical formula with examples, however collectively they simplify the accounting of the overall chain of echo formation into a final histogram. Consequently, the issues of complex interference phasors are not included in the analysis. In this sense our analysis returns to the earliest formulations of weak scattering from cylinders (Rayleigh, 1918b; Albini and Nagelberg, 1962).

The applicability of this framework in different soft tissues or organs in normal vascularized tissue remains to be more widely tested. Furthermore, the important task of diagnosing abnormalities is left for further research. Presumably a disruption of the normal vascular structure in aggressive cancers would change the power law b and the vessel number density N_0 , but a detailed study of these and other common pathologies are beyond the scope of this paper.

Further high resolution studies of the vasculature in 3D for different organs, along with corresponding high resolution B-scans of the same organs, would be helpful for testing and refining this theoretical framework of speckle amplitudes from soft vascularized tissues.

ACKNOWLEDGEMENTS

This work was supported by National Institutes of Health grant number R21EB02590. The author is grateful to Ph.D. students Juvenal Ormachea and Jihye Baek for providing envelope data for analysis, and to Terry Swanson of Pfizer Inc., Groton CT, for providing the superb B-scan of the rat liver.

APPENDIX: MAPPING AND TRANSFORMATION OF FUNCTIONS

Herein we consider how the size distribution of cylindrical elements determines a distribution of echoes, in order to derive a histogram of echo amplitudes. A lucid explanation of the mapping of distributions is given in Chapter 5 of Papoulis (1987). This is explained in terms of probability density functions, where a new variable is defined by $y = g(x)$, and x is a random variable with known probability density function $f(x)$. However, the results hold for all well-behaved analytic functions where the area under the curve within any small interval is preserved by the mapping. We also assume a single valued mapping of $y = g(x)$ and its inverse

$x = g^{-1}(y)$ for simplicity. In that case, by simply equating equal areas under some region of x_0 to $x_0 + \Delta x$, and mapping that to the y variable, the transformation rule is:

$$f_y(y) = \frac{f_x(x)}{|dg(x)/dx|}, \quad (12)$$

where on the right side the inverse function $x = g^{-1}(y)$ is then used to eliminate x as a variable and produce an equation in terms of y . The concept is illustrated in **Figure A1**.

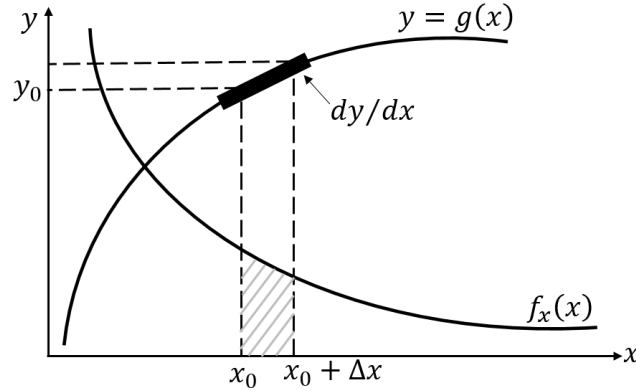


Figure A1. Schematic illustration following Papoulis showing the distribution of one continuous variable x with a distribution $f_x(x)$ which is mapped to a new distribution where $y = g(x)$, and retaining the area under the curve.

An important feature of this transformation for echo envelope functions emerges as a dramatic consequence, for anywhere near to a local maxima where the first derivative of the envelope approaches zero, the denominator term in eqn (12) approaches zero and the transformation produces a singularity around that point. Thus, as we apply this to echo envelopes where x is the echo space or time variable and y is the echo envelope, each local maxima creates a large spike in the histogram of the envelope.

As an example, let $y = A_0(1 - x^2)$ for $-1 < x < 1$. By symmetry, we only need to consider $0 < x < 1$ and assume uniform likelihood of sampling within this interval so $f_x(x) = 1$. Also,

$|dy/dx| = A \cdot 2x$ and $x = g^{-1}(y) = \sqrt{1 - (y/A_0)}$. Finally, from eqn (12), $f(y) = 1/\left[2\sqrt{1 - (y/A)}\right]$

for $0 < y < A$, which has a singularity as $y \rightarrow 1$ (the value of the local maximum of $y = f(x)$).

This is illustrated in **Figure A2** below for $A_0 = 1$.

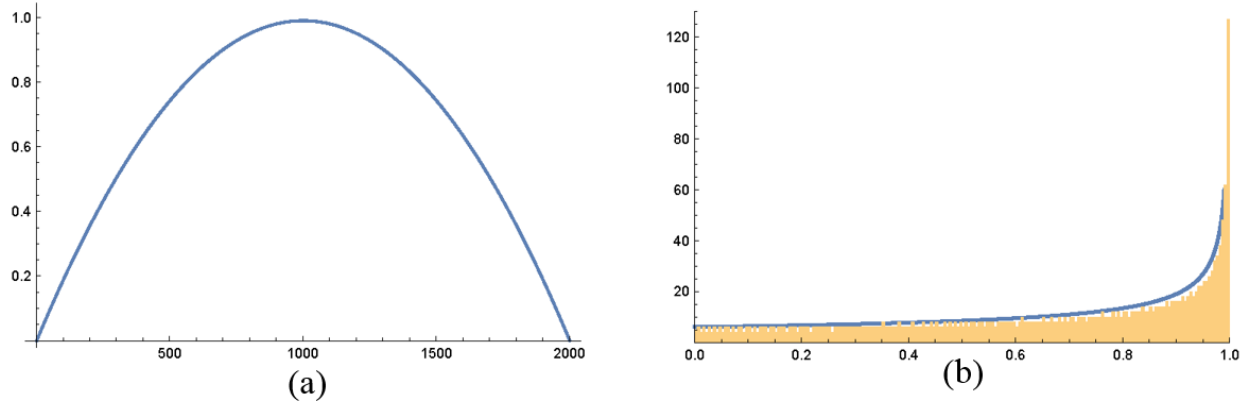


Figure A2. Example of sampling an envelope function (a) to produce a resulting histogram (b) and theory from eqn (12) (solid line). In (a), the vertical axis is amplitude, maximum value normalized to 1; the horizontal axis is time or distance, arbitrary units. In (b), the vertical axis is sampled counts in a histogram; the horizontal axis is echo amplitude. Note the spike near amplitude=1, the local maximum of the envelope.

Another example of a modified Gaussian is shown in **Figure A3**, where $y = e^{-x^2/2}(1 - x^2)$, producing a similar result deriving from the singularity produced by the local maximum of the envelope function.

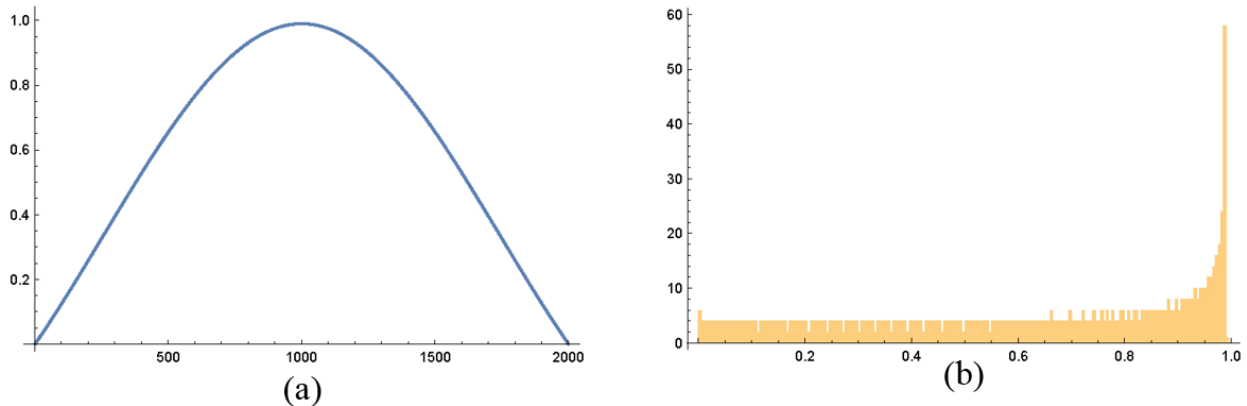


Figure A3. Second example using a modified Gaussian envelope in (a) and the resulting histogram in (b), demonstrating the dominant value or singularity mapped from the local maximum. In (a), the vertical axis is amplitude, maximum value normalized to 1; the horizontal axis is time or distance, arbitrary units. In (b), the vertical axis is sampled counts in a histogram; the horizontal axis is echo amplitude. Note the spike near amplitude=1, the local maximum of the envelope.

Thus, we conclude that the histogram of envelopes contains a dominant contribution formed by the local maximum, where the first derivative approaches zero. This dominant contribution from the local maximum of the echo is also assumed to be proportional to the RMS echo amplitude formed by convolution, eqn (6), and then is used in the superposition or summation over all cylinder sizes in our formulation.

REFERENCES

- Abramowitz, M., and Stegun, I. A. (1964). *Handbook of mathematical functions with formulas, graphs, and mathematical tables* (U.S. Govt. Print. Off., Washington,).
- Albini, F. A., and Nagelberg, E. R. (1962). "Scattering of a plane wave by an infinite inhomogeneous, dielectric cylinder—an application of the Born approximation," *J Appl Phys* **33**, 1706-1713.
- Bamber, J. C., and Dickinson, R. J. (1980). "Ultrasonic B-scanning: a computer simulation," *Phys Med Biol* **25**, 463-479.
- Bracewell, R. N. (1965a). *The Fourier transform and its applications, Chapter 8* (McGraw-Hill, New York).
- Bracewell, R. N. (1965b). *The Fourier transform and its applications, Chapter 12* (McGraw-Hill, New York).
- Burckhardt, C. B. (1978). "Speckle in ultrasound B-mode scans," *IEEE Trans Sonics Ultrason* **25**, 1-6.
- Campbell, J. A., and Waag, R. C. (1984). "Measurements of calf liver ultrasonic differential and total scattering cross sections," *J Acoust Soc Am* **75**, 603-611.

- Cramblitt, R. M., and Parker, K. J. (1999). "Generation of non-Rayleigh speckle distributions using marked regularity models," IEEE Trans Ultrason Ferroelectr Freq Control **46**, 867-874.
- Gore, J. C., and Leeman, S. (1977). "Ultrasonic backscattering from human tissue: a realistic model," Phys Med Biol **22**, 317-326.
- Kutay, M. A., Petropulu, A. P., and Piccoli, C. W. (2001). "On modeling biomedical ultrasound RF echoes using a power-law shot-noise model," IEEE Trans Ultrason Ferroelectr Freq Control **48**, 953-968.
- Kutay, M. A., Petropulu, A. P., and Piccoli, C. W. (2003). "Breast tissue characterization based on modeling of ultrasonic echoes using the power-law shot noise model," Pattern Recogn Lett **24**, 741-756.
- Landini, L., and Verrazzani, L. (1990). "Spectral characterization of tissues microstructure by ultrasounds: a stochastic approach," IEEE Trans Ultrason Ferroelectr Freq Control **37**, 448-456.
- Laporte, C., Clark, J. J., and Arbel, T. (2009). "Generalized poisson 3-D scatterer distributions," IEEE Trans Ultrason Ferroelectr Freq Control **56**, 410-414.
- Macovski, A. (1983). *Basic Ultrasonic Imaging* (Prentice-Hall, Englewood Cliffs, N.J.).
- Morse, P. M., and Ingard, K. U. (1987). *Theoretical Acoustics, Chapter 8* (Princeton University Press, Princeton, NJ).
- Papoulis, A. (1987). *The Fourier integral and its applications* (McGraw-Hill, New York), 11.
- Parker, K. J. (2016). "The H-scan format for classification of ultrasound scattering," J OMICS Radiol **5**, 1000236.

- Parker, K. J. (2019). "Shapes and distributions of soft tissue scatterers," *Phys Med Biol*, <https://doi.org/10.1088/1361-6560/ab2485>.
- Parker, K. J., Carroll-Nellenback, J. J., and Wood, R. W. (2019). "The 3D spatial autocorrelation of the branching fractal vasculature," *Acoustics* **1**, 369-381.
- Poularikas, A. D. (2010). "Transforms and applications handbook, Chapter 6," in *The electrical engineering handbook series* (CRC Press, Boca Raton), p. 7.21.
- Prince, J. L., and Links, J. M. (2015). *Medical imaging signals and systems* (Pearson, Boston).
- Rayleigh, L. (1897). "XXXVII. On the passage of waves through apertures in plane screens, and allied problems," *Philos Mag* **43**, 259-272.
- Rayleigh, L. (1918a). "On the scattering of light spherical shells, and by complete spheres of periodic structure, when the refractivity is small," *Proceedings of the Royal Society of London. Series A* **94**, 296-300.
- Rayleigh, L. (1918b). "XLI. The dispersal of light by a dielectric cylinder," *The London, Edinburgh, and Dublin Philosophical Magazine and Journal of Science* **36**, 365-376.
- Sleepe, G. E., and Lele, P. P. (1988). "Tissue characterization based on scatterer number density estimation," *IEEE Trans Ultrason Ferroelectr Freq Control* **35**, 749-757.
- Thijssen, J. M. (2003). "Ultrasonic speckle formation, analysis and processing applied to tissue characterization," *Pattern Recogn Lett* **24**, 659-675.
- Tuthill, T. A., Sperry, R. H., and Parker, K. J. (1988). "Deviations from Rayleigh statistics in ultrasonic speckle," *Ultrason Imaging* **10**, 81-89.
- Wear, K. A., Wagner, R. F., Brown, D. G., and Insana, M. F. (1997). "Statistical properties of estimates of signal-to-noise ratio and number of scatterers per resolution cell," *J Acoust Soc Am* **102**, 635-641.

Zagzebski, J. A., Lu, Z. F., and Yao, L. X. (1993). "Quantitative ultrasound imaging: in vivo results in normal liver," *Ultrason Imaging* **15**, 335-351.